Journal of Applied Physics

RESEARCH ARTICLE | AUGUST 02 2024

Mode transitions in a magnetically shielded Hall thruster. II. Stability criterion

Benjamin A. Jorns ; Matthew Byrne ; Parker Roberts ; Leanne Su ; Ethan Dale ; Richard R. Hofer

Check for updates

J. Appl. Phys. 136, 053302 (2024)
https://doi.org/10.1063/5.0205985

View Online
Export Citation

05 August 2024 14:30:42

Nanotechnology & Materials Science
Optics & Photonics
Impedance Analysis
Scanning Probe Microscopy
Sensors
Failure Analysis & Semiconductors

Unlock the Full Spectrum.
From DC to 8.5 GHz.
Your Application. Measured.
Find out more
Zurich Instruments

AIP Publishing

Journal of Applied Physics ARTICLE pubs.aip.org/aip/jap

Mode transitions in a magnetically shielded Hall thruster. II. Stability criterion

Cite as: J. Appl. Phys. **136**, 053302 (2024); doi: 10.1063/5.0205985
Submitted: 28 February 2024 · Accepted: 10 July 2024 ·
Published Online: 2 August 2024

View Online Export Citation CrossMark

Benjamin A. Jorns,[1,a)] Matthew Byrne,[1] Parker Roberts,[1] Leanne Su,[1] Ethan Dale,[1] and Richard R. Hofer[2]

AFFILIATIONS

[1]Department of Aerospace Engineering, University of Michigan, Ann Arbor, Michigan 48109, USA
[2]Jet Propulsion Laboratory, California Institute of Technology, Pasadena, California 91011, USA

[a)]**Author to whom correspondence should be addressed:** bjorns@umich.edu

ABSTRACT

A stability criterion is derived for mode transitions in the discharge current oscillations of a magnetically shielded Hall thruster. The two-equation model evaluated in Paper I for these large-amplitude (>100% background), low-frequency (<25 kHz) current oscillations is generalized and then validated with measurements from a 9 kW class test article. It is shown that the model can re-create quantitatively trends in both oscillation amplitude and frequency with discharge voltage and current. The validated model is non-dimensionalized and applied to derive an analytical stability criterion for the onset of large-amplitude oscillations. The resulting expression depends on several properties, including discharge current, discharge voltage, neutral transit time in the channel, length of the acceleration zone, magnetic field strength, and channel area. The criterion is leveraged to inform two mitigation strategies—changing magnetic field strength and controlling anode temperature— for adjusting the stability margin of the thruster. The criterion is also employed to motivate a physical explanation for why mode transitions occur and, in turn, why the stability margin differs between shielded and unshielded thrusters.

05 August 2024 14:30:42

© 2024 Author(s). All article content, except where otherwise noted, is licensed under a Creative Commons Attribution-NonCommercial-NoDerivs 4.0 International (CC BY-NC-ND) license (https://creativecommons.org/licenses/by-nc-nd/4.0/). https://doi.org/10.1063/5.0205985

I. INTRODUCTION

Mode transitions in power and discharge current oscillations are a common occurrence in Hall effect thrusters. These axisymmetric plasma devices are widely leveraged for propellant-efficient but low-thrust propulsion in space. Their mode transitions are characterized by shifts from relatively quiescent operation to states with large-scale oscillations in the plasma properties. While these transitions have been the subject of extensive study in more traditional, "unshielded" Hall thrusters,[1–28] the introduction of a new variant of thruster design, "magnetically shielded," has led to the discovery of a mode shift not previously observed.[29,30]

Shielded thrusters employ a unique magnetic field configuration to mitigate the dominant erosion process in these devices—the sputtering of the channel that confines the main discharge. The subsequent increase in the thruster lifetime with shielding[31–33] is a key enabler for employing Hall thrusters for deep-space, long duration robotic missions. With that said, it has been found that when shielded thrusters designed for a nominal discharge current are operated at the high specific impulse desirable for deep-space missions, >2500 s, but at 60% of their nominal operating current, they undergo a mode transition to a highly oscillatory state. This is characterized by large-amplitude (>100% background) and low-frequency (~10–50 kHz) oscillations in the discharge current and total power. The onset of this mode poses a particular risk for mission profiles that call for the spacecraft to spiral from the sun. As the solar power available falls, the discharge current may drop sufficiently to lead to a mode transition, which, in turn, may adversely impact thruster life.

The goal of this two-part series is to characterize and model this new mode transition for the purpose of identifying stability criterion and mitigation strategies. In the first part of this work, we experimentally evaluated a model for the current oscillations exhibited by this mode. This effort was guided by the observation that the relatively low frequency and large amplitude are commensurate

with the canonical breathing mode exhibited in unshielded Hall thrusters. The breathing mode is conventionally believed to be related to periodic ionization in the thruster channel (cf. Ref. 1). Working under the assumption that the mode in the shielded thruster is based on the same effect, we applied the two-equation, two-zone model for the discharge current and neutral density oscillations in unshielded thrusters originally proposed by Barral and Peradzyński.[6] We, in turn, used direct experimental measurements of the time-resolved plasma properties inside the channel of a Hall thruster to demonstrate that the simplifying assumptions for this model were valid for a single operating condition, 300 V discharge voltage and 3 kW discharge power. We also showed this model was able to re-create the amplitude and relative phasing of oscillations in neutral density and discharge current.

Informed by these experimental observations, we discussed in this previous work the de-stabilizing mechanism for the oscillations. Physically, fluctuations in current in the downstream "acceleration zone" of the thruster—characterized by where ion velocity rapidly increases—are communicated upstream nearly instantaneously (on the timescale of the oscillation) to an "ionization zone." The changing current in this upstream region impacts the local ionization rate of neutrals. The resulting perturbations in neutral density require some time to propagate downstream to the acceleration zone where they can either reinforce or interfere with the ongoing oscillations, thus promoting instability.

The key parameters that influence the relative phasing of the oscillations—the ionization frequency and transit time—are both functions of the steady-state operation of the thruster, i.e., its voltage, current, etc. This dependence suggests that the criterion for constructive interference and, thus, the onset of the oscillations will vary with operating conditions. Given that the model presented in Paper I depends on these key plasma properties, it invites the possibility that the model may be able to re-create mode transitions with changing discharge current and voltage. However, this previous work only focused on a single operating state of a shielded thruster, and its extensibility remains an open question.

In Paper II of this study, we examine parametrically the validity of the model from Paper I as a function of operating condition and leverage the validated model to find a stability criterion for the mode transition. To this end, this paper is organized in the following way. In Sec. II, we review the key governing equations for the model that were introduced in Paper I and then apply common scaling law arguments to relate these governing equations to the typical operating conditions of a Hall thruster. In Sec. III, we describe the experimental setup for parametrically characterizing the mode transition in a shielded thruster. In Sec. IV, we compare experimental measurements of discharge current oscillations to the model predictions to evaluate its validity and extensibility. For Sec. V, we employ our model to motivate an analytical stability criterion for the onset of the mode transition. In Sec. VI, we examine the dependence of this stability criterion on design and operating conditions of the thruster. For Sec. VII, we explore experimentally mitigation strategies for the mode transition that are motivated by the derived stability criterion. In Sec. VIII, we discuss the limitations and implications of our results.

II. REVIEW OF MODEL FOR DISCHARGE CURRENT OSCILLATIONS

We review in this section the model from Paper I based on the work of Barral and Peradzyński.[6] We, in turn, convert this model to a form that can be related to the standard set of operating conditions that are typically prescribed for a Hall thruster experiment.

A. Governing equations

We show in Fig. 1 the cross section for the channel of a canonical Hall thruster. This system, which has azimuthal symmetry, consists of an axial electric field, $\vec{E}$, originating from an upstream anode applied transverse to a radial magnetic field, $\vec{B}$. During steady-state operation, neutral gas flows from a manifold in the anode and is impact ionized by electrons trapped in an azimuthal $E \times B$ drift. The ions resulting from this ionization, which are sufficiently massive that they are unmagnetized, are accelerated by the electric field axially and out of the geometry.

We identify two separate zones for describing the dynamics of the oscillations in the channel: an ionization zone and an acceleration zone. The acceleration zone is defined in the context of this work as the region where the ion speed most rapidly increases. It is correlated with the peak electric field and electron temperature in the thruster. We define the ionization zone as the region upstream of the acceleration zone where the majority of ionization occurs. We note, however, that moderate ionization can also occur in the acceleration zone.

We adopt the model we presented in Paper I to describe the oscillations in this channel geometry.[34] It consists of two equations for the total discharge current and the volumetrically averaged neutral density in the acceleration zone,

$$\frac{dI}{dt} = (1 - c)I\bar{\beta}[N - \bar{N}], \tag{1}$$

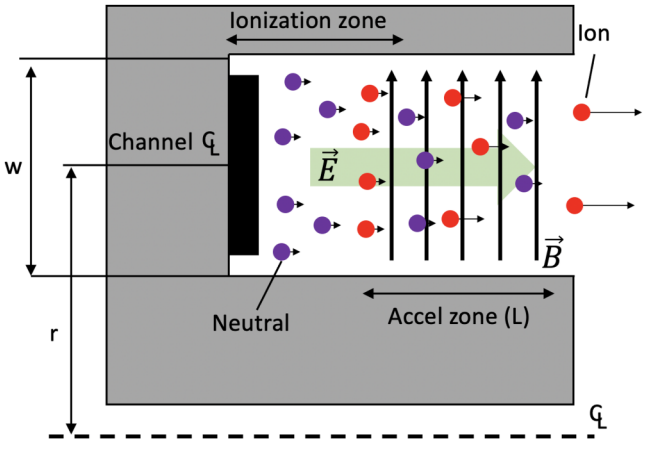

FIG. 1. Cross section of the Hall thruster canonical geometry.

05 August 2024 14:30:42

© Author(s) 2024

$$\frac{dN}{dt} = -\bar{\gamma}NI + \frac{Q_0}{L}\exp\left[-\bar{\gamma}\int_{t-\tau}^{t} I(t^*)dt^*\right]. \quad (2)$$

Here, $\bar{x}$ denotes the time-average of quantity x, I is the discharge current, N is the neutral density averaged volumetrically over the acceleration zone, β denotes the rate coefficient for ionization averaged spatially over the acceleration zone, $\bar{\gamma} = \bar{\beta}(\bar{n}/\bar{I})$ is the volumetric "effective" ionization rate of neutrals in the acceleration zone, where n is the volumetrically averaged plasma density, Q_0 denotes the volumetric flow rate of neutrals from the anode, L is the length of the acceleration zone, τ is the transit time of neutrals across the ionization zone to the acceleration zone, and c is a constant of order unity that was found to be approximately $c = 0.5$ in Paper I. This constant stems from the fact that it was shown in Paper I that the magnitude of fluctuations in neutral density is reduced by anti-correlated fluctuations in the relative drift between the electron and ion species.

The relation in Eq. (1) indicates that the rate of increase in current in the discharge channel is driven by fluctuations in the rate of creation of charge carriers, i.e., ionization. This ionization is assumed to be dominated by variations in the neutral density and total discharge current. Equation (2) shows that the change in the neutral density in the acceleration zone is the result of two competing effects: flux of neutrals into the acceleration zone from the upstream ionization region (second term on right-hand side) and the rate of depletion of neutrals due to ionization (first term). The analytical form of the flux of neutrals from upstream is formulated to represent the time-dependent depletion of this species from ionization as they transit the ionization zone. The rate of this depletion depends on both the dwell time of the neutrals, τ, and the number of charge carriers in this region, proportional to I.

Physically, in this model, the variations in the discharge current driven by the fluctuations in the acceleration zone can be communicated "instantaneously" upstream to the ionization region. This is ensured by current continuity in the channel and the relatively high mobility of the electrons. This change in current, which is correlated with fluctuations in the plasma density, results in perturbations in the neutral density in the ionization region. These fluctuations then require some time to propagate to the acceleration zone. The resulting delay between inlet neutral density oscillations and discharge current oscillations can lead to positive feedback, reinforcing the instability and promoting growth.

B. Relating model parameters to thruster operating parameters

To perform a comparison of the model described in Eqs. (1) and (2) to measurements of oscillations in a Hall thruster, we invoke a series of simplifications that express the parameters in the governing equations in terms of common Hall thruster operating conditions:

- The average electron temperature in the acceleration zone is proportional to the discharge voltage:[35] $\bar{T}_e = \Gamma V_D$, where Γ is a constant of order 0.1. We, thus, can express the rate coefficient, which is a function of electron temperature, $\bar{\beta} = \bar{\beta}(\Gamma V_D)$.
- We invoke a simplified Ohm's law, neglecting the role of electron pressure, to represent the average electron drift speed in the acceleration zone: $\bar{u}_e = -(V_D/L)B_0^{-1}\Omega_e^{-1}$, where Ω_e denotes the electron Hall parameter (assumed to be much greater than unity) and B_0 is the magnitude of the average magnetic field.
- The ion speed in the acceleration zone scales with the accelerating voltage, $\bar{u}_i = c_0\sqrt{2qV_D/m_i}$, where q is fundamental charge, m_i denotes the ion mass, and c_0 is a constant. This latter constant, which is less than unity, accounts for the fact that ions are still accelerating in this region and have not experienced the full applied potential.
- The ratio of the time-averaged density to discharge current in the acceleration zone can be approximated as $\bar{n}/\bar{I} = 1/(qA(\bar{u}_i - \bar{u}_e))$, where A is the area of the channel.
- We can relate the discharge current to the inlet flow rate $\eta_b\bar{I} = Q_0Aq$, where η_b denotes the beam utilization efficiency. We have neglected the role of multiply charged ions in this equivalence and invoked the assumption from Paper I that the flux of neutrals downstream of the acceleration zone is negligible compared to the inlet flux from the anode.
- The neutral transit time is a function of the speed of neutrals emerging from the anode, which is assumed to be thermal: $\tau \propto \sqrt{T_n}$ where T_n is the neutral temperature. To estimate the scaling for the neutral temperature, we assume that the dominant mechanism heating the anode is power absorbed from the discharge, which scales with the electron temperature and the discharge current:[35] $P_a \propto \bar{T}_e\bar{I} \propto V_D\bar{I}$. The anode temperature is the most elevated in the thruster, with a value typically exceeding 400 °C[36] and where heat is primarily rejected through radiation. We, thus, approximate, $P_a \propto T_n^4$. With this last relation, we have $T_n \propto (V_D\bar{I})^{1/4}$ such that $\tau = \tau_{ref}(P_{ref}/(V_D\bar{I}))^{1/8}$, where τ_{ref} denotes the transit time at a reference power.

Subject to these assumptions and invoking the steady-state forms of Eqs. (1) and (2), we can write for the constants in these relations,

$$\bar{\gamma} = \frac{\bar{\beta}(\Gamma V_D)}{qA(c_0\sqrt{2qV_D/m_i} + (V_D/L)B_0^{-1}\Omega_e^{-1})}, \qquad \bar{N} = \frac{\eta_b}{qAL\bar{\gamma}}e^{-\tau_{ref}(P_{ref}/(V_D\bar{I}))^{1/8}\bar{\gamma}\bar{I}}. \quad (3)$$

These results depend on four properties that are experimentally controlled: the discharge voltage, the average discharge current, the cross-sectional area of the channel, and the magnetic field strength. There are additional model parameters (η_b, Γ, L, τ_{ref}, P_{ref}, c_0, Ω_e), which are not necessarily known a priori. We can motivate typical values for these, however, based on general scaling laws for Hall thrusters and our measurements from Paper I. To this end, we show in Table I the model parameters we assumed to be fixed for this analysis.

For the coefficient between the electron temperature and voltage, it has been shown that the peak electron temperature in Hall thrusters scales approximately as $\Gamma = 0.1$ (cf. Ref. 35). However, the temperature in the acceleration zone can vary by an order of magnitude from this peak value. Since we consider the spatial average over the length of the acceleration zone in the model, we introduce a factor of 1/2 to the peak electron

05 August 2024 14:30:42

© Author(s) 2024

TABLE I. Model parameters for the two-equation model.

Γ	0.05	Scaling between temperature and discharge voltage
L	1 cm	Acceleration zone length
c_0	0.25	Scaling factor for ion speed in acceleration zone
η_b	0.85	Beam utilization efficiency
τ_{ref}	21 μs	Neutral transit time of ionization zone at 3 kW
P_{ref}	3 kW	Power where transit time was inferred

temperature scaling: $\Gamma = 0.05$. This value is consistent with our experimental measurements reported in Paper I.

For the acceleration length, we adopt $L = 1$ cm, which is informed by experimental measurements of the acceleration zone from Paper I. We note these that this is not the equivalent to the length of the thruster channel but rather is driven by experimental observations of the spatial extent of this zone. We employ $c_0 = 0.25$ for the scaling factor of the ion speed in the acceleration zone, which is motivated by our experimental observation of the average ion speed in the acceleration zone from Paper I. We use a value of $\eta_b = 0.85$ for the beam utilization. This choice also is based on previous experimental measurements, where it has been shown to be approximately constant over a wide range of throttling conditions.[37] We adopt values of $\tau_{ref} = 21\,\mu$s and $P_{ref} = 3$ kW for the neutral dynamic calculation. These too are based on Paper I where we examined a thruster operating at 3 kW and inferred the transit time by comparing the model predictions for oscillations in the inlet flow to the acceleration zone to experimental measurements.

Armed with these results, there is one remaining parameter in our model prescription, Ω_e. In practice, the nature of this Hall parameter, which represents an effective cross field transport coefficient for the electrons, remains an open area of investigation.[38] In lieu of prescribing a value for it in this work, we, thus, leave it as a free parameter. We, subsequently, employ regression analysis to determine whether there are values for the Hall parameter that allow the two-equation model to capture the experimentally observed variation in oscillation properties with operating conditions.

Before proceeding with this analysis, we note that although we have elected to assume fixed values for the parameters shown in Table I, some of the properties, such as acceleration zone length, L, are relatively poorly defined and subject to the qualitative interpretation of the data. We estimate, for example, approximately 20% uncertainty in our determination of this length. In principle, we could allow for this variance by treating these model parameters as variable and regressing them simultaneously with the Hall parameter against experimental data. We have elected not to adopt this approach in this analysis in the interest of simplicity: our overarching initial goal is simply to determine whether there are physically plausible parameter combinations where the model can re-create trends in the experimental data. Provided this validation is demonstrated, we can be confident in leveraging the model to attempt to find a stability criterion. This criterion then is formulated in such a way (Secs. V–VII) that the values of the model parameters are not assumed and can be varied. The resulting stability criterion, thus, generalizes the model, and we subsequently explore the sensitivity of the criterion to the parameters in Table I in Sec. VI.

With that said, to hedge against the possibility that the initial validation we report in the following is highly sensitive to the specific values in Table I, we allowed each of these parameters to vary by 20% and performed the same single-parameter regression of the Hall parameter. We were able to find qualitatively similar findings as those reported in the following. There was comparable agreement between modeling and experiment, and the regressed Hall parameters were within a factor of 2.

C. Numerical implementation

In the following analysis, we investigate predictions for oscillations in discharge current from the model outlined in Eqs. (1) and (2) as a function of average voltage and current. To this end, we outline here our numerical approach to solving these equations. First, we prescribed the magnetic field strength, B_0, and the area of the thruster channel, A, based on the test article size. We then set values for the discharge voltage, V_D, and average discharge current, $\bar{I}$. These are dictated by the experimental operating condition of interest to which we are attempting to compare. We then prescribed the model parameters (η_b, Γ, L, τ_{ref}, P_{ref}, c_0), based on the values given in Table I and assumed a value for Ω_e.

With a fixed set of operating and model parameters, we determined the constants in Eqs. (1) and (2) from the relationships given in Eq. (3). We then used initial conditions for the discharge current based on the average values: $I(t = 0) = \bar{I}$, $N(t = 0) = \bar{N}$ and numerically evaluated the governing equations with the NDSolve package in Wolfram's Mathematica for 2 ms of time. This is at a factor of twenty times longer than the anticipated period of the simulated oscillations. From these numerical solutions, we generated predictions for the time-resolved discharge current, $I(t)$. We then applied the same Fourier and peak-to-peak analysis to this numerical product as for the experimental results (see Sec. III D). This allowed for a direct comparison with experimental observations.

We remark here that we found through a parametric study over initial conditions (0–300% of the prescribed average values of, $\bar{I}$, $\bar{N}$) that the long-time behavior of the numerical solutions, as quantified by the amplitude and frequency of the oscillations, was independent of initial conditions. This is consistent with the interpretation that these non-linear relations support one dominant mode.

Armed with this numerical prescription, a key goal in the following analysis is to determine for each combination of average discharge voltage and discharge current if there is a numerical solution from the governing equations that re-creates experimental measurement. We investigate this by systematically varying the one free model parameter, Ω_e, in an effort to match data. We also consider parametrically the response of the model when this parameter is assumed to be constant.

III. EXPERIMENTAL SETUP

For our experimental campaign, we measured the frequency spectra and amplitudes of discharge current oscillations in a magnetically shielded Hall thruster over a wide range of voltages and discharge currents. We describe in the following the thruster, the facility, and the key diagnostics and metrics.

05 August 2024 14:30:42

© Author(s) 2024

A. Thruster

We employed the H9 Hall thruster shown in Fig. 2 for this investigation.[39,40] This laboratory thruster was jointly developed by the Jet Propulsion Laboratory, University of Michigan, and the Air Force Research Laboratory and shares design heritage with the Hall Effect Rocket with Magnetic Shielding (HERMeS) developed by NASA.[30] Nominally a 9 kW class device, the H9's throttling range is approximately 0.6–12 kW discharge power, 1000–3000 s specific impulse, and 50–500 mN thrust. This engine employs a plasma lens magnetic field topography, a centrally mounted lanthanum hexaboride (LaB6) cathode, and a high-uniformity gas distributor/anode assembly. Long-life is achieved with magnetic shielding, graphite pole piece covers, a graphite cathode keeper, and the use of a cathode-tied electrical configuration that connects the thruster body to the cathode common. At $V_D = 600$ V and 9 kW, thrust, total specific impulse, and total efficiency of the H9 are 436 mN, 2690 s, and 63%, respectively. The H9's operation has been characterized extensively on xenon and krypton with measurements of performance and internal plasma properties.[41–47] For the tests reported in this study, we varied the discharge voltage and current while maintaining a constant magnetic field strength and a flow rate to the cathode that was 7% of the anode mass flow rate.

B. Facility

We performed our tests in the Alec D. Gallimore Large Vacuum Test Facility (LVTF) at the University of Michigan.[48] The LVTF is a 6 m diameter, 9 m long stainless steel vacuum chamber equipped with 19 cryogenic pumps to achieve xenon pumping speeds >550 kl/s. For this campaign, we measured the background pressure with an ion gauge mounted in the exit plane of the thruster approximately 1 m from the thruster's outer diameter.[49] For the maximum flow rates in this campaign, ∼15 mg/s of xenon, the facility pressure, as measured by the ionization gauge and corrected for xenon, did not exceed 5×10^{-6} Torr.

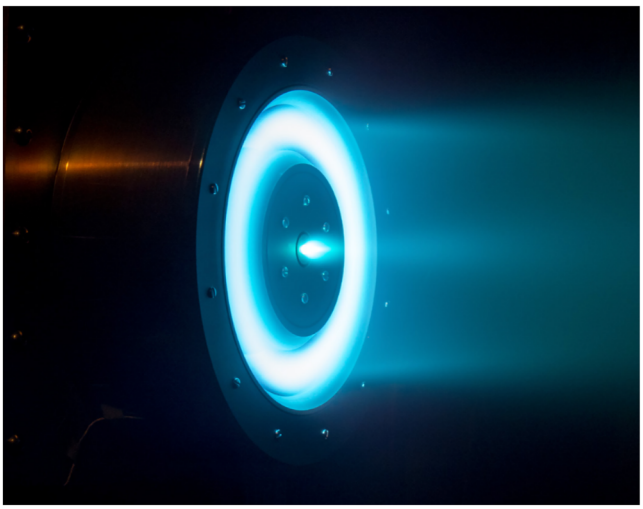

FIG. 2. Image of the H9 Hall effect thruster operating at 300 V and 15 A.

The discharge power was provided by a constant voltage power supply placed in series with a discharge filter to protect the supply from large-scale transients. This filter consisted of an RLC circuit comprised of a 100 Ω resistor, 47 uF capacitor, and 0.3 mH inductor. Power to the thruster's electromagnets was provided by a pair of TDK-Lambda Power Supplies. Xenon propellant flow was moderated by a pair of calibrated flow controllers. The thruster's operation and health were controlled and monitored with an optically isolated telemetry system that logged measurements of key data including the DC discharge voltage, mass flow rate, and DC discharge current.

C. High-speed current probe

The primary diagnostic we employed for this campaign was a high-speed current sensor connected to the anode side of the discharge supply line between the discharge filter and the thruster. We also monitored the cathode line current and transients in the voltage to the thruster. These latter two showed quantitative agreement with the anode line in terms of relative amplitude and frequency of oscillations. For brevity, we do not report these measurements here. For all cases, the sampling rate was 625 kHz with 62 kilosamples. Before making each measurement at a given operating condition, we ran the thruster until the mean discharge current, $\bar{I}$, achieved a steady-state value.

D. Metrics for characterizing current oscillations

In this study, we focused on characterizing two spectral features of the discharge oscillations as a function of the operating condition: the relative amplitude and frequency. To represent the former, we adopted the relative peak-to-peak amplitude (RPK). We evaluated this metric by dividing both the experimental and model-based time-resolved data into N time series of length $\Delta t \sim 200\,\mu$s. We then defined

$$\mathrm{RPK} = \frac{100\%}{N} \frac{\sum_{j=1}^{N} \left(I_{\max(j)} - I_{\min(j)} \right)}{I_D}, \tag{4}$$

where $I_{\max(j)}$ and $I_{\min(j)}$ denote the maximum and minimum of the current oscillation in the jth time series, respectively.

We analyzed the power spectrum of the oscillations to identify the dominant frequency, $f_{\max}$. As we note in the following, there were experimental configurations in which the dominant oscillation was not the low-frequency breathing mode but rather a higher frequency oscillation not modeled by our simplified theory. In these cases, there was still a lower amplitude mode consistent with the breathing mode frequency. We denoted the frequency of this oscillation as f_{BM}.

IV. RESULTS OF PARAMETRIC EXPERIMENTAL STUDY AND COMPARISON TO MODEL

We present in this section the properties of the discharge current oscillations in the H9 thruster as a function of the operating condition. We, in turn, compare these properties to the outputs of the two-equation model. To this end, we first consider the $V_D = 600$ V (high specific impulse) state at two discharge currents.

05 August 2024 14:30:42

© Author(s) 2024

This comparison illustrates the mode transition. We then expand the study to include a parametric investigation over a range of voltages and currents.

A. Mode transition at 600 V

As a first step in investigating the nature of the mode transition in the shielded thruster, we highlight in this section an example of the oscillations shifting from large amplitudes to a quiescent state. We show in Fig. 3 experimental measurements (black) for the time-dependent variations in current [Figs. 3(a) and 3(b)] and the power spectra [Figs. 3(c) and 3(d)] for two operating conditions, $\bar{I} = 7.5$ A and $\bar{I} = 15$ A, at a discharge voltage of $V_D = 600$ V. From the experimental results, we see that at $\bar{I} = 7.5$ A, the thruster exhibits a coherent and large-amplitude (RPK $> 100\%$) oscillation with a fundamental frequency of $f_{\max} = 15$ kHz. The harmonics in the spectrum above 15 kHz [Fig. 3(c)] indicate its cnoidal nature. These nonlinear features combined with the low-frequency of the oscillation are typical of the canonical breathing mode.[50]

At the higher discharge current, $\bar{I} = 15$ A, the experimental power spectrum [Fig. 3(d)] still exhibits a peak at $f_{BM} = 15$ kHz, which is commensurate with the breathing mode, but the amplitude is six orders of magnitude smaller. This is too low to be observed in the raw time-resolved signal. There is a more

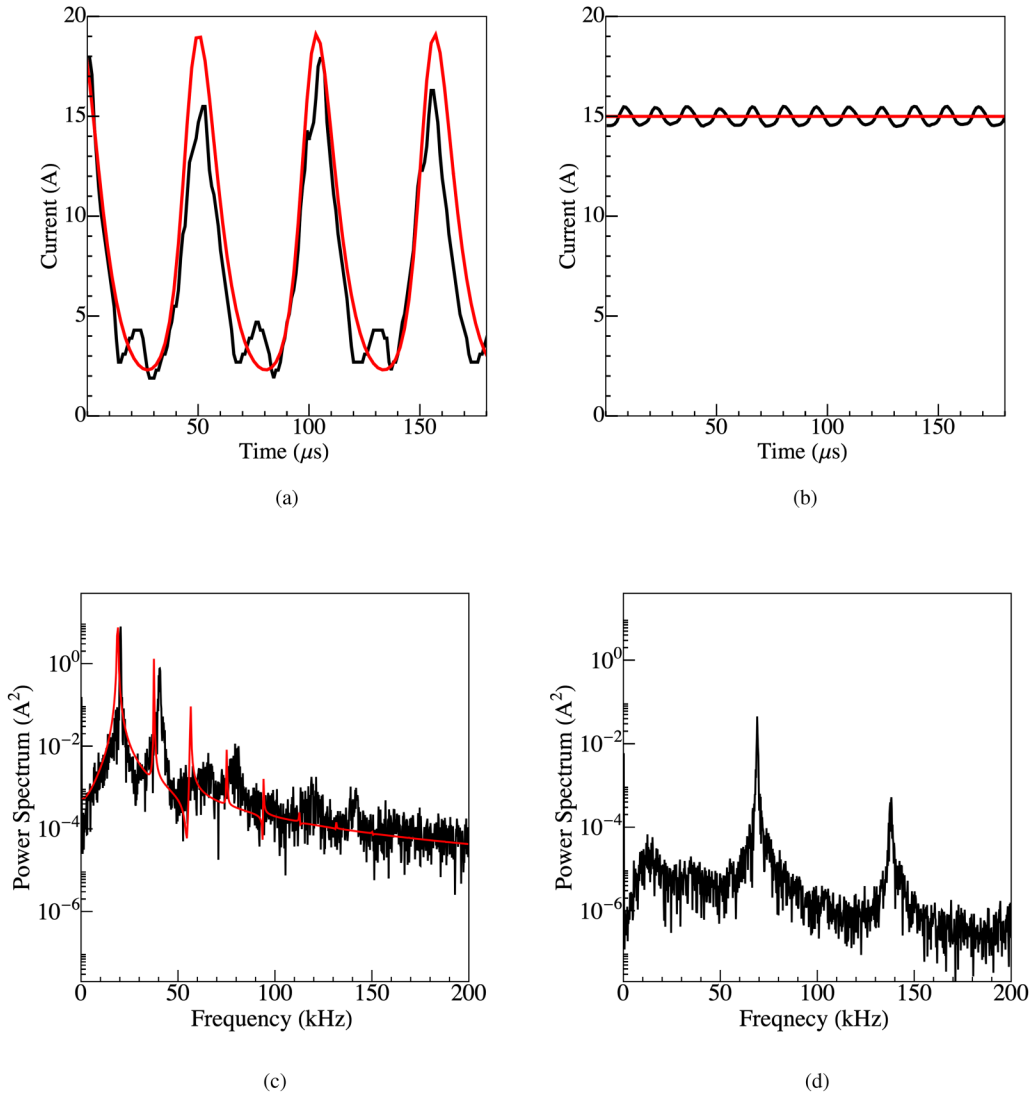

FIG. 3. (a) Measured (black) and modeled (red) discharge current oscillations in time at (a) $V_D = 600$ V and $\bar{I} = 7.5$ A and (b) $V_D = 600$ V and $\bar{I} = 15$ A. Measured (black) and modeled (red) power spectra of discharge current oscillations at (c) $V_D = 600$ V and $\bar{I} = 7.5$ A and (d) $V_D = 600$ V and $\bar{I} = 15$ A. The model result for the power spectrum is not shown for (d) as the oscillation level is negligible at this level. The Hall parameter assumed for the model is $\Omega_e = 800$ for both current conditions.

05 August 2024 14:30:42

© Author(s) 2024

prominent oscillation with a dominant frequency of $f_{max} = 70$ kHz. This is manifest as a rapid fluctuation in the time-resolved signal [Fig. 3(b)] with an order of magnitude lower amplitude than the breathing mode exhibited at $\bar{I} = 7.5$ A. This higher frequency instability is fundamentally different than the breathing mode and has been shown in magnetically shielded thrusters to be associated with a rotational cathode wave.[26,45,51] Taken together, the experimental results from $\bar{I} = 7.5$ A and $\bar{I} = 15$ A show that the breathing mode is damped, and higher frequency oscillations dominate the discharge at a higher current.

For comparison, we show in Fig. 3 the model-based solutions (red) from Eqs. (1) and (2) with constants given by Eq. (3) evaluated from the values in Table I and assuming $V_D = 600$ V and $\bar{I} = 7.5$ A [Figs. 3(a) and 3(c)] and 15 A [Figs. 3(b) and 3(d)]. For each numerical solution, we assumed a Hall parameter of $\Omega_e = 800$. This value is of the same order of magnitude inferred in previous experimental and theoretical treatments of the H9 at this operating condition.[52] It is evident from the results shown in Fig. 3 that the two-equation model with this assumed value of the Hall parameter is able to recreate the time-dependent behavior of the large-scale oscillation exhibited experimentally at the $\bar{I} = 7.5$ A condition. The amplitude matches the experiment, and the dominant frequency of oscillation agrees within 1 kHz. The spectrum similarly exhibits harmonics of the dominant frequency with decaying behavior consistent with the experimental result. At $\bar{I} = 15$ A, the model correctly re-creates the effective damping of the breathing mode. This is represented by the non-oscillatory current and the absence of content in the power spectrum. We note that the model does not capture the higher frequency oscillation exhibited by the experimental data at $\bar{I} = 15$ A. This, however, is because the underlying physics of this simple model cannot represent the rotational cathode mode—a distinct phenomenon. Leaving this discrepancy aside, the results exhibited in Fig. 3 provide preliminary validation of the model's capability to represent the mode transition of interest. Indeed, the only free parameter we adjusted to achieve this agreement was Ω_e, and the value we found that yielded the model prediction with the best agreement was in line with previous experimental measurements.

B. Parametric study over operating conditions

In an extension of the results from Sec. IV A, we performed a parametric study of the oscillations over the operating envelope of the thruster. We varied the discharge voltage and current in 50 V and 1 A increments, respectively, and measured the properties of the discharge current fluctuations. We, in turn, employed the global metrics of RPK and f_{max} (Sec. III D) to collapse the oscillation properties into scalar quantities.

1. Experimental measurement

We show in Fig. 4(a) a contour plot of the RPK in oscillations as a function of discharge current and voltage. From this result, we see that for discharge voltages above $V_D = 400$ V, there is a range of currents, $\bar{I} = 10$–12 A, below which the thruster transitions from a region of low oscillations (RPK $< 50\%$) to high amplitude (RPK $> 100\%$). This transition is consistent with the result shown for the $V_D = 600$ V case in Fig. 3(a). Below $V_D = 350$ V, however, a transition to instability does not onset for the range of currents interrogated.

We note here that in a departure from our analysis in Paper I where we analyzed the high amplitude oscillations at $V_D = 300$ V and $\bar{I} = 10$ A to guide our model development, Fig. 4(a) shows that this condition is relatively quiescent. This can be ascribed to the fact that we employed a different, off-nominal magnetic field strength for the study performed in Ref. 43 that, in turn, formed the basis of the data reported in Paper I. In this former case, we deliberately adjusted the magnetic field to achieve an oscillatory state. This was to facilitate the diagnostic technique of that particular study. In the results reported here, we have employed a magnetic field 25% stronger, which evidently allowed for more stability at this operating condition. We return to a discussion of the role of the magnetic field, which is always important in Hall thrusters, in Secs. VI and VII.

We show in Fig. 4(b) the dominant frequency, f_{max}, from the experimentally measured power spectra of the discharge current oscillations. This result indicates a transition from highly oscillatory conditions dominated by the lower, breathing mode frequency, $f_{max} \approx 10-20$ kHz, to a state exhibiting the higher frequency cathode oscillation, $f_{max} \approx 70$ kHz. This shift in the dominant frequency mirrors the trends in the RPK amplitude oscillations [Fig. 4(a)]. Most saliently, the RPK $= 100\%$ contour in Fig. 4(a) approximately follows the contour in Fig. 4(b) where there is an evident shift in frequency. In our subsequent analysis with our model, we, thus, use the value RPK $= 100\%$ as the criterion to denote a mode transition. This threshold is marked by the bolded contour line in Fig. 4(a).

As a final metric, we show in Fig. 4(c) the breathing mode frequency, f_{BM}, recalling that this mode persists in all cases but with a decrease in the amplitude [cf. Fig. 3(d)]. This result suggests that for average discharge currents below $\bar{I} = 12.5$ A, the breathing mode frequency increases with both voltage and current. However, the relative change in the magnitude is minor, with frequencies ranging from ~10 kHz at the lower end of the parameter space to 19 kHz at the upper end. Beyond $\bar{I} = 12.5$ A, the trends are not as immediately evident, but this may in part be attributed to the fact that the breathing mode is largely damped at these higher currents and thus poorly defined. Indeed, the frequency peak associated with the lower frequency mode becomes progressively broader as the cathode oscillation becomes more prevalent at higher currents [Fig. 3(d)].

2. Comparison to model

We apply here the model for comparison with experimental measurements. As discussed in Sec. II, we solved Eqs. (1) and (2) at each combination of voltage and current following the prescription outlined in Sec. II C. In order to make the most favorable comparison between simulation and experiment, at each voltage and current condition, we evaluated the model for Hall parameters of $\Omega_e = 100$–1000, a range consistent with previous experimental measurements of the H9.[52] For each Hall parameter in this range, we extracted the RPK from the simulation as well as the frequency of the oscillation, f_{BM}, and calculated a weighted residual with the experimental measurements of RPK and f_{BM}. Figure 5 shows the

05 August 2024 14:30:42

© Author(s) 2024

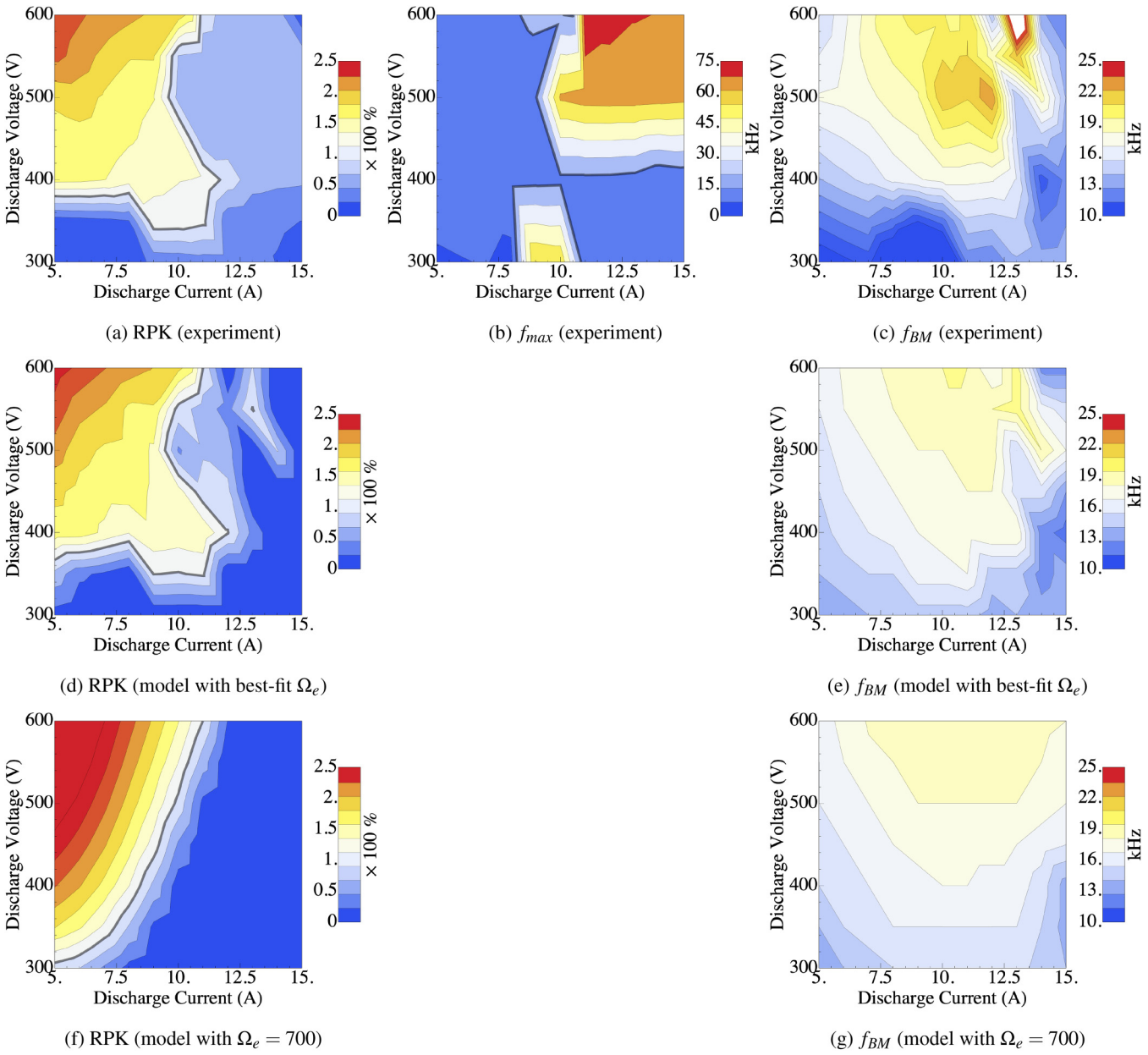

FIG. 4. Experimental and model results for relative peak-to-peak (RPK) maximum frequency of oscillation, f_{max}, and frequency of oscillation associated with the breathing mode, f_{BM}. For modeling results, the figures show the cases where Ω_e was allowed to vary to yield the best-fit with the experimental data and where it was fixed. Bolded contours on (a), (d), and (e) denote the 100% fluctuation level, while in (b), it denotes the mode transition in frequency. Linear interpolation was employed to generate these figures. (a) RPK (experiment), (b) f_{max} (experiment), (c) f_{BM} (experiment), (d) RPK (model with best-fit Ω_e), (e) f_{BM} (model with best-fit Ω_e), (f) RPK (model with $\Omega_e = 700$), and (e) f_{BM} (model with $\Omega_e = 700$).

values of Ω_e that yielded the lowest residual for each voltage and current combination. Figures 4(d) and 4(e) illustrate the results for the RPK and f_{BM} yielded by the model when using the values of Ω_e at each voltage and current from Fig. 5. We note here that $f_{max} = f_{BM}$ for the modeling results as the governing equations are unable to resolve the high frequency cathode mode (Sec. IV A).

We first remark on the quantitative agreement between the two-equation model and the experimental measurement over the

05 August 2024 14:30:42

© Author(s) 2024

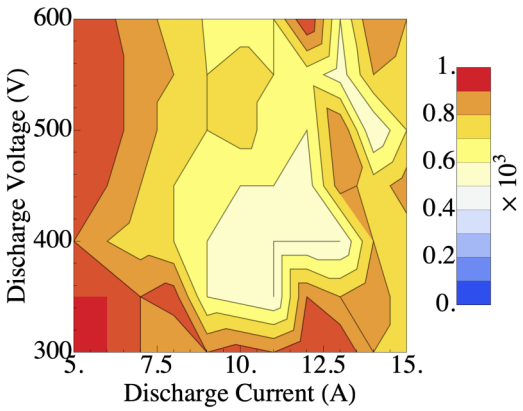

FIG. 5. Hall parameter, Ω_e, that yielded the lowest residual between model and experiment for each voltage and current.

parameter space. With only one free parameter, Ω_e, the model is able to capture the transition to instability as well as the relative amplitude of oscillations [Fig. 4(d)]. Similarly, the model predictions reflect the trends in the frequency of the breathing mode [Fig. 4(e)], showing the same structure in which the frequency generally increases with voltage and current with non-monotonic features at the highest currents and voltages. Taken together, these features illustrate that the simple model has the flexibility to represent the measured mode transitions. This, thus, demonstrates extensibility beyond the limited conditions under which we originally validated it in Paper I.

In practice, the predictive capability of the model is curtailed by the fact that we calibrated the Hall parameter as a function of voltage and current. With that said, as shown in Fig. 5, the variation in the best-fit Hall parameters over the domain was only a factor of two: $\Omega_e = 500$–900, a range of values within an order of magnitude of previous measurements inferred from the H9.[52] This relatively minor variation suggests that the model predictions may only be weakly dependent on the Hall parameter. To examine this possibility, we show in the final row in Fig. 4 the RPK and frequency predictions for the model when we assume the median value of the Hall parameter from Fig. 5, $\Omega_e = 700$.

As can be seen, the fidelity of the model comparison with the experiment suffers when a fixed value of the Hall parameter is employed. Both the RPK and frequency predictions lose the detail that is exhibited when Ω_e is allowed to vary. The transition to instability at fixed voltage, for example, appears more relaxed—occurring over 1–2 A instead of the ∼0.5 A as found with the experimental result. This departure suggests that the electron mobility as represented by the Hall parameter has a role at least in the starkness of the onset of the transition. With that said, using an average, typical value of the Hall parameter does still yield trends that qualitatively capture key features exhibited by the data. For example, the trends in most of the contours for the oscillation level remain qualitatively the same between model and experiment for voltages above $V_D = 400$ V. Similarly, the qualitative changes in the frequency are also anticipated with a fixed Hall parameter.

In summary, the previous findings underscore that the two-equation model has sufficient fidelity to represent mode transitions. Moreover, the model exhibits a "predictive" capability in so much as when run with an average value for its one free parameter, it is able to predict a qualitatively correct threshold for stability and the variation in the dominant frequency. We note here as well that we repeated the above analysis but allowing for different assumed values for perhaps the least well-characterized model parameter in the table, the model length. We changed the assumed length from L = 0.8–1.2 cm. In these cases, we were able to identify values for the Hall parameter as a function of voltage and current that still yielded predictions with the same features shown in the second row of Fig. 4. Moreover, the average value for these Hall parameters for each of these cases only varied by approximately 20%. Armed with this validation, we turn in Sec. V to leveraging this model to derive a stability criterion for the onset of the mode transition.

V. DERIVATION OF STABILITY CRITERION

The overarching goal in finding an analytical stability criterion is to relate the properties of the thruster operation to conditions for when the mode transition is anticipated. To this end, a common approach to stability analysis for dynamical equations of the form shown in Eqs. (1) and (2) is to linearize and to search for solutions in complex space with positive imaginary components.[6,10,53] This method has limited utility for our system, however, given that the dynamics of the oscillations are non-linear. For this work then, we instead adopt an alternative, semi-empirical approach. This leverages the fact that for set constants in the governing equations, the oscillations always converge to the most unstable mode (Sec. II C). This occurs regardless of the initial conditions.

With this in mind, we first non-dimensionalize the variables in Eqs. (1) and (2) by defining the following relations:

$$\hat{t} = t\bar{N}\bar{\beta}; \quad \hat{N} = \frac{N}{\bar{N}}; \quad \hat{I} = I\frac{\bar{\gamma}}{\bar{\beta}\bar{N}}. \tag{5}$$

In the first term, we have normalized the time by the average ionization frequency of ions in the acceleration zone. In the second term, we have normalized the neutral density in the acceleration zone by the steady-state neutral density. In the third relation, we have normalized the discharge current by a quantity that depends on the ratio of the effective ionization rate to the ionization frequency of ions. This latter term can also be expressed as $\hat{I} = (I/\bar{I})\alpha_{iz}$ where α_{iz} is the average ionization fraction in the acceleration zone.

Armed with these definitions, Eqs. (1) and (2) reduce to

$$\frac{d\hat{I}}{d\hat{t}} = (1-c)\hat{I}(\hat{N}-1), \tag{6}$$

$$\frac{d\hat{N}}{d\hat{t}} = -\hat{I}\hat{N} + \hat{\bar{I}}\exp\left[-\left(\int_{\hat{t}-\hat{\tau}}^{\hat{t}}(\hat{I}-\hat{\bar{I}})d\hat{t}\right)\right], \tag{7}$$

where we have defined $\bar{\tau} = \tau\bar{N}\bar{\beta}$ as the normalized neutral transit time and introduced the parameter $\hat{\bar{I}}$ that approximately corresponds to the time-averaged, normalized discharge current.

05 August 2024 14:30:42

© Author(s) 2024

The normalized expressions in Eqs. (6) and (7) show that the dynamics are driven only by two non-dimensional parameters: the normalized average discharge current and the normalized neutral transit time. We can leverage this fact to vary these non-dimensional parameters and search for empirical relationships for when the mode transition occurs. With this in mind, we show in Fig. 6 the RPK inferred from numerical solutions of Eqs. (6) and (7) as a function of these two non-dimensional quantities.

The key features from Fig. 6 are the well-defined contours, which represent constant relative peak–peak amplitude for the oscillations. From the arrangement of these contours, we see that for fixed normalized discharge current, the system becomes progressively more oscillatory with longer transit times. Conversely, with fixed normalized transit time, the transition to instability occurs with increasing normalized discharge current. We, in turn, can identify from this result a contour corresponding to 100% RPK, which we have defined as the criterion for mode transition. By inspection, we see that this contour can be described with an empirical fit,

$$\hat{\tau}\hat{\bar{I}}^{2/5} > 2.9. \tag{8}$$

In non-dimensional terms, this inequality represents the stability criterion for the mode transition. We can return this to dimensional coordinates to find

$$\tau(\bar{\beta}\bar{N})^{3/5}(\bar{I}\bar{\gamma})^{2/5} > 2.9. \tag{9}$$

This result when used in conjunction with Eq. (3) provides a prescription for relating the operating conditions of the thruster—discharge voltage and discharge current—as well as parameters such as magnetic field strength and area to the onset criterion of the instability. In Sec. VI, we leverage this expression to explore parametrically how the stability threshold can be changed by altering these properties.

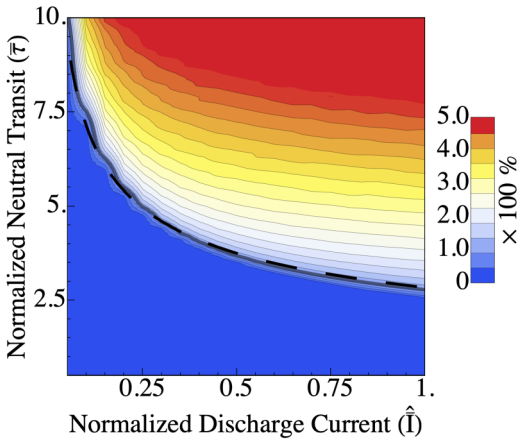

FIG. 6. Relative peak-to-peak (RPK) oscillations as a function of normalized discharge current and transit time. The contour corresponding to 100% oscillation is highlighted with a bold line. The empirical fit [Eq. (8)] is shown as a dashed line.

VI. PARAMETRIC DEPENDENCE OF STABILITY CRITERIA ON OPERATING CONDITIONS

We have focused in Sec. IV on the stability of the thruster as a function of two canonically controlled operating conditions, the discharge voltage and discharge current. This was manifest as a line demarcated where the fluctuations exceed 100% peak to peak (Fig. 4). The criterion derived in Eq. (9) suggests that changing other properties of the thruster can influence the locations in the operational space of voltage and current where instability occurs. With this in mind, we examine in this section the impact of neutral transit time, acceleration zone length, magnetic field strength, and channel area on the stability margin of the thruster.

To this end, we first establish a baseline stability margin for our experimental setup. We use the same constants as shown in Eq. (3) along with the values given in Table I to numerically evaluate Eq. (9) as a function of voltage and current. We also have assumed the average value of $\Omega_e = 700$. We show these results as the black lines in Fig. 7. The regions to the right of the curves are stable whereas the regions to the left are unstable. Notably, the lines are commensurate with the 100% threshold contour shown in Fig. 4(f), providing a check on the validity of the expression we derived from our non-dimensional analysis.

In Fig. 7(a), we show the result when we keep all parameters constant but allow the reference neutral transit time, τ_{ref} to vary. Figure 7(b) shows the change when we allow the length of the acceleration zone to vary. Figure 7(c) illustrates the impact of varying magnetic field strength. In addition, Fig. 7(d) indicates the influence of the channel area.

All four results illustrate the fact that the stability threshold is sensitive to these aspects of thruster operation. The dependence on neutral transit time suggests that shorter residence improves the stability margin—the curve shifts to the upper left quadrant such that more voltage and current combinations are stable. Similarly, longer acceleration zones and stronger magnetic fields improve the stability margin for the thruster. We note here that this latter dependence—the fact that increasing magnetic field improves thruster stability has been remarked upon in a wide range of experimental studies (cf. Ref. 54). Finally, we see that a smaller channel area, and, thus, higher effective discharge current density, appears to improve the stability margin.

The physical principles underlying these dependencies on thruster configuration are nuanced but broadly can be attributed to the fact that changing these properties alters the relative timing between ionization in the acceleration zone and the rate at which neutrals in the ionization zone are depleted and enter the acceleration zone. As we discussed in Paper I and Sec. II, the constructive interference or phasing of these effects dictates the magnitude of the instability. We return to this point in Sec. VIII A.

VII. MITIGATION STRATEGIES INFORMED BY STABILITY CRITERION

The parametric plots in the previous section have shown that the stability threshold in voltage-current space can be adjusted by changing other aspects of the thruster geometry and operation. We leverage these results in this section to explore as a proof-of-concept two mitigation strategies for the H9: adjusting the

05 August 2024 14:30:42

© Author(s) 2024

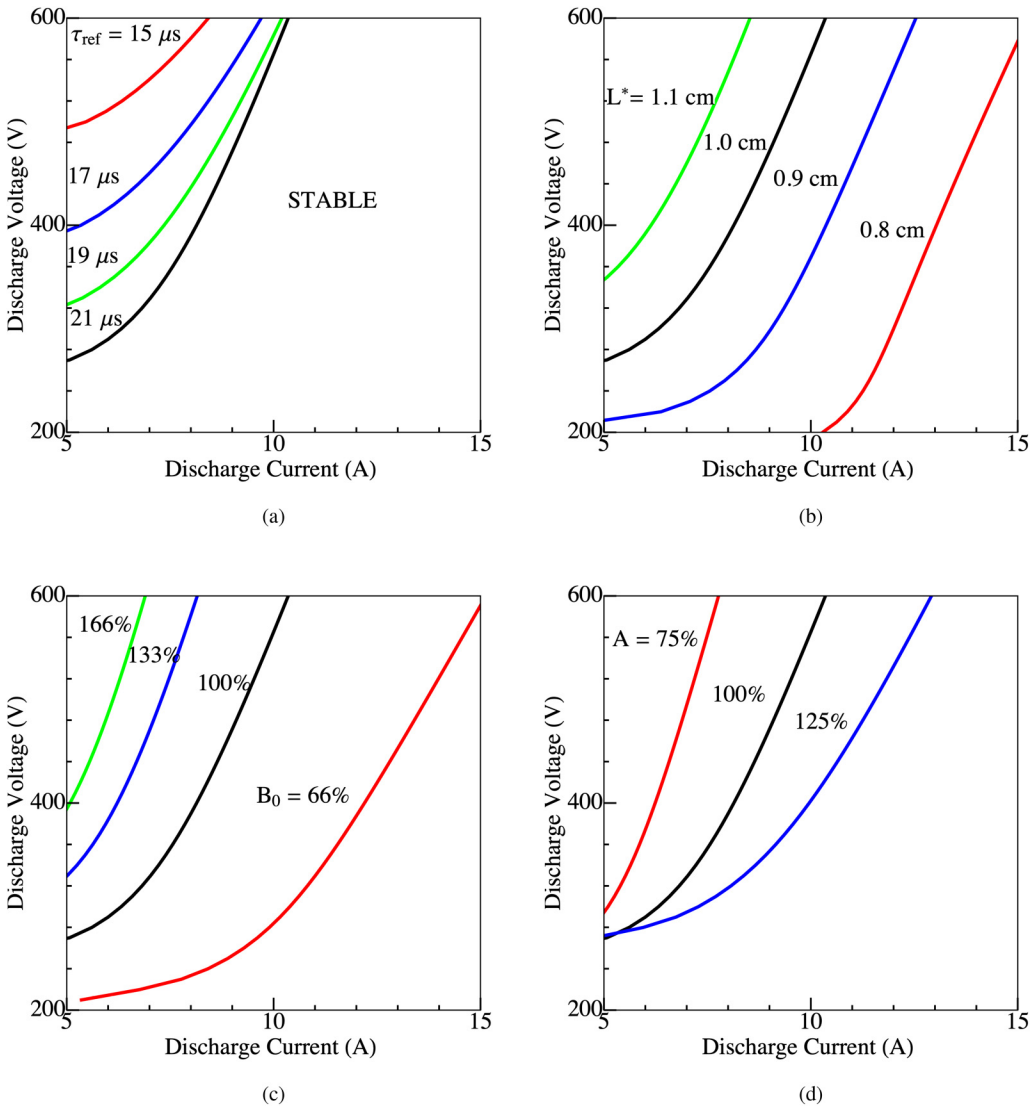

FIG. 7. Stability threshold as a function of discharge and current for variable (a) reference neutral transit time at 3 kW, τ_{ref}, (b) acceleration zone length, L, (c) magnetic field magnitude, B_0, and (d) channel area, A. The regions to the right of the curves represent where oscillation levels, RPK, are below 100%. The threshold is based on evaluating Eq. (9) with constants given by Eq. (3) and values from Table I.

magnetic field strength [informed by Fig. 7(c)] and manipulating the transit time [informed by Fig. 7(a)].

The role of magnetic field strength has been shown in previous work to have a direct influence on thruster stability.[54] Indeed, it generally is understood, consistent with our predictions exhibited by Fig. 7(c), that increasing magnetic field strength reduces the magnitude of thruster breathing mode oscillations. In order to assess the influence of this parameter on the stability margin for the H9, we repeated the stability study at $V_D = 600$ V as a function of current at three applied magnetic field strengths—$B_0 = 87.5\%$, 100%, and 112.5%. Figure 8(a) shows these results where we have denoted the 100% RPK fluctuation level with a horizontal dashed line. As can be seen, the increase in the magnetic field strength to $B_0 = 112.5\%$ yielded the anticipated result: the transition point moved to a lower discharge current by approximately 1.5 A. On the other hand, decreasing the magnetic field strength $B_0 = 87.5\%$ *also* moved the stability threshold to lower currents. This is a departure from the first-order theoretical prediction from Fig. 7(c).

This deviation at reduced magnetic field strength may not entirely be attributed to the failings of the theory. It has been shown, for example, that decreasing the magnetic field can lead to an effective downstream shift and lengthening of the acceleration

05 August 2024 14:30:42

© Author(s) 2024

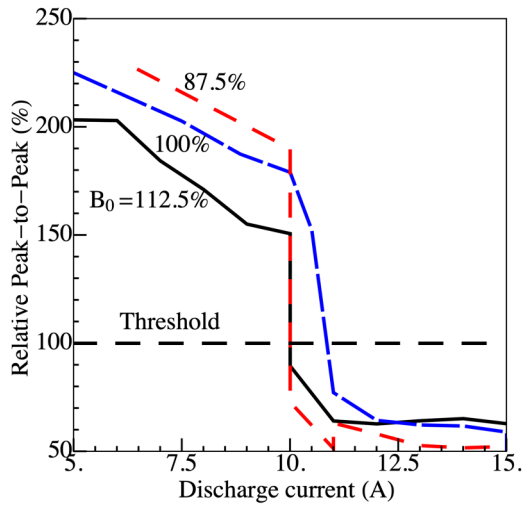

(a)

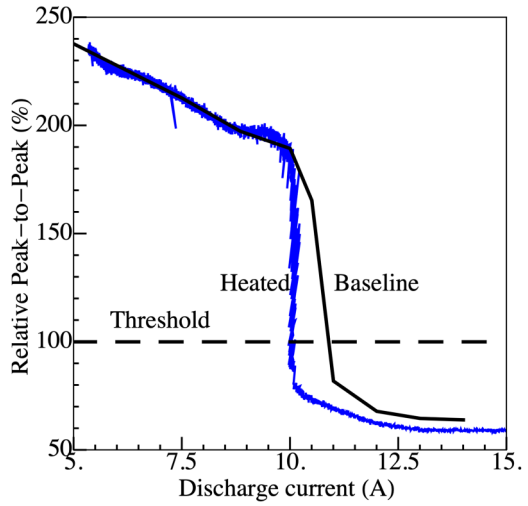

(b)

FIG. 8. Response of thruster stability with (a) varying magnetic field strength and (b) heated anode with $V_D = 600$ V.

zone.[55–58] In turn, Fig. 7(b) shows that a more relaxed acceleration zone, as represented by L, can shift the stability margin to a lower current. It is, thus, possible that the trade between lengthening of the acceleration zone and increasing the magnetic field strength combine to lead to a non-monotonic response in the stability threshold to the magnetic field. To this point, we note that previous studies on unshielded thrusters have shown there is a minimum in current oscillations with field strength.[54] After achieving a minimum in RPK by increasing the magnetic field, raising this field further can lead to moderate increases in the RPK. With that said, we ultimately cannot be conclusive about these arguments absent direct measurements of how the acceleration zone length in the H9 changes with field strength.

The discussion from the preceding section suggests another strategy for modifying the transition to instability: adjusting the reference neutral transit time, τ_{ref}. Per Fig. 7(a), decreasing this parameter can shift the stability margin to allow for stable operation at higher voltages and lower currents. To assess this possibility experimentally, we recall (Sec. II B) that we derived our expression for neutral transit time by assuming equilibrium between the power fluxing to the anode and radiation from the anode surface. Given that we have found the thermal equilibrium timescale for the thruster to be on the order of minutes, we can artificially decrease the effective reference residence time, τ_{ref}, by running the thruster at a higher power, hotter condition and then rapidly reducing the current. To this end, we operated the H9 at its maximum power, $V_D = 600$ V and $\bar{I} = 15$ A, for 3 h. We then rapidly decreased the current over 30 s from $\bar{I} = 15$ A to $\bar{I} = 5$ A by lowering the anode flow rate and monitoring the discharge current oscillations with a high-speed data acquisition card.

We show in Fig. 8(b) the results of this study where we plot the RPK as a function of discharge current for the baseline and heated anode cases. The shift in current is qualitatively consistent with Fig. 7(a) in which we predicted the transition point would move to a lower current. We cannot directly compare the two results as we did not have measurements of anode temperature. However, this figure does suggest that adjusting neutral transit time by changing the anode temperature is a possible viable mechanism for controlling the mode transition. To this point, previous experimental studies have shown that anode cooling, i.e., increasing neutral transit time, has caused higher levels of oscillations in unshielded thrusters, a result anticipated by our analysis.[59]

In summary, these experimental results show that it is possible to effect change on the stability margin of a shielded thruster at high voltage by adjusting its operating conditions.

VIII. DISCUSSION

We discuss here several aspects of the preceding experimental and numerical work. First, we leverage our normalized stability criterion to expand on the physical interpretation we presented in Paper I and Sec. II for the mechanisms governing the onset of the instability. We then discuss the implications of our results for understanding the presence of this mode transition in shielded thrusters as opposed to unshielded thrusters. We conclude with a discussion of efforts to mitigate the transition to instability and possible implications for ground testing efforts.

A. Physical interpretation of stability criterion

In our discussion of the simplified model evaluated in Paper I, we argued that in order to promote the mode transition, it was necessary to have a mechanism originating from a spatially distinct region of the thruster, the ionization zone, to provide positive feedback to reinforce the ionization oscillations in the acceleration zone. This interpretation is consistent with the larger body of work on the breathing mode oscillation where it has been suggested that this mode is inherently greater than zero-dimensional.[6,8,15,16,60]

05 August 2024 14:30:42

© Author(s) 2024

To this end, following Barral and Peradzyński,[6] we have treated the thruster as two 0D regions where the dominant properties that oscillate on the timescale of the breathing mode are the discharge current and neutral density. The 0D regions in the thruster are causally connected by two processes: (1) the time-dependent flux of neutrals from the upstream ionization region to the downstream acceleration zone and (2) changes in discharge current driven by ionization in the acceleration zone communicated "instantaneously" (on the timescale of the breathing mode) by the electron motion upstream to the ionization zone. The fluctuations in neutrals in the ionization zone that result from ionization induced by variations in the discharge current can lead to a positive feedback loop, reinforcing variations in neutral density in the downstream acceleration zone. These fluctuations can constructively interfere to promote growth of the instability. The conditions for where positive growth occurs ultimately are dictated by the timescales of ionization and neutral transit.

The stability criterion we derived in Eq. (9) reflects this interpretation quantitatively, showing explicitly the dependence on ionization and neutral transit timescales. Indeed, we can re-write this criterion as

$$\tau \nu_{iz} > 2.9(\alpha_{iz})^{3/5}, \tag{10}$$

where ν_{iz} denotes the ionization rate of neutrals. Physically, this result suggests that if the ionization rate is small compared to the neutral transit time, i.e., $\tau \nu_{iz} \ll 1$, the neutral density has only slight modulation before entering the acceleration zone. The downstream boundary of the ionization zone becomes the equivalent to the steady-state flow emerging from the anode. There, thus, is no mechanism for positive feedback in oscillations from the ionization region upstream. Rather, the system converts to the case with a steady influx of neutral density, which is unconditionally stable.[60] Conversely, if the neutral transit time is long compared to the ionization time scale, there is sufficient time for the neutral density to be modulated before entering the acceleration zone, thus promoting the possibility of positive feedback. In practice, the mechanisms that influence the ionization time as well as ionization fraction depend on several aspects of the thruster including magnetic field strength, current, discharge voltage, acceleration zone length, and channel area. These dependencies are illustrated by the parametric studies presented in Fig. 7.

B. Contrast between shielded and unshielded thrusters

A motivating question behind this study is why shielded thrusters exhibit a mode transition to instability at high discharge voltage and low current, whereas unshielded thrusters previously have not. Our key assertion from Paper I is that the oscillations in the shielded thrusters are still a manifestation of the canonical breathing mode in Hall thrusters. It is not a unique instability to shielded devices. It, therefore, follows that the difference between shielded and unshielded thrusters must be attributed to differences in where the stability threshold occurs in the operating space of the device.

With this in mind, there are at least two variations between shielded and unshielded thrusters that might shift the stability threshold. For example, as shown in Fig. 7(a), decreasing the neutral transit time can lead to improvement in the stability margin. As an artifact of their design, magnetically shielded thrusters displace the acceleration zone downstream compared to unshielded thrusters.[33] As a result, the effective length from the anode to acceleration zone increases. This may lead to a longer neutral transit time, which in the context of Fig. 7(a) could shift the stability margin for shielded thrusters to higher currents when compared to unshielded thrusters.

Another factor to consider is the role of acceleration zone length. As Fig 7(c) shows, as this parameter increases, the stability margin also improves. The influence of shielding on acceleration zone length is not immediately evident, although as discussed in the preceding, shielding has the effect of displacing the acceleration zone downstream of the thruster channel. This shift may also be correlated with a variation in zone length, although we have limited experimental evidence to quantify this effect.

Ultimately, while these trends offer possible explanations for the difference in the mode transition between these two thruster variants, we cannot point conclusively to one cause. Indeed, it is expected that all the parameters in our model will be influenced by the shift from shielded to unshielded, and it is the convolution of these effects that may explain the departure in stability margins. Directly measuring the model parameters between the two thruster variants would provide additional insight into this question.

C. Implications for thruster testing and mitigation

The dependencies of the stability criterion on the operating condition highlighted in Sec. VI may have implications for testing and development efforts. For example, our preceding work has shown how neutral transit time may be a critical feature in determining the stability of the thruster. This invites practical questions about the role of the thruster thermal state in effecting the oscillation level. It is a common practice to operate Hall thrusters for several hours after initial exposure to vacuum conditions in order to outgas the discharge channel walls. As part of this outgassing process, contaminants (usually water) are released. This is correlated with an artificial increase in the average discharge current and is often associated with higher amplitude oscillations (cf. Ref. 61). The oscillation level subsequently decreases over time.

While outgassing ultimately may be correlated with high amplitude breathing mode oscillations, our work suggests a parallel and complementary interpretation. As the thruster is operated, the temperature of the channel and anode increase. As we have shown in the preceding, this will reduce neutral transit time and, for a given operating condition, may reduce the amplitude of oscillations. In addition to eliminating contaminants then, it may be the thermal soaking that also helps improve thruster stability during the initial outgassing period.

This dependence on temperature may have implications for transitioning to orbit as well. Indeed, the heat rejection in space may be different than test facilities in such a way that ultimately may lead to steady-state temperatures of the thruster channel and anode that differ from the ground test. This, in turn, may impact the stability margin for a given operating condition in orbit.

05 August 2024 14:30:42

© Author(s) 2024

In terms of mitigation, we have noted in the preceding, Sec. VI, how the stability margin in principle may be improved by opting for higher anode temperatures, providing more magnetic field margin, or decreasing the effective acceleration zone length. We note though that these parameters are often convolved in the thruster implementation and may not be changed in isolation. As a final comment, we remark here about an additional mitigation strategy we were not able to examine in this work: adjusting current density by decreasing the channel area. Indeed, a notable finding from our analysis [Fig. 7(d)] is that a higher effective *current density* that results from a smaller area channel may improve the stability margin. To this point, the influence of this parameter was observed in a recent experimental campaign in which the current density to a design variant of the H9 was increased by a factor of ten compared to its nominal value.[37] The thruster in this case showed a marked reduction in RPK at these elevated levels. While this was a positive proof of concept, we note that this particular mitigation strategy has the potential negative impact of promoting higher wall losses and, thus, lowering thruster efficiency.

IX. CONCLUSION

We focused in this work on deriving a stability criterion for mode transitions in a magnetically shielded Hall thruster. This effort was motivated by the observation that shielded thrusters exhibit a transition to an oscillatory state at high specific impulse (discharge voltage) and low current. We based this investigation on the two-equation model presented in Paper I for oscillations in thruster discharge current.

We parametrically evaluated this model against experimental data from a magnetically shielded Hall thruster and showed that it could represent observed experimental trends in current oscillations. We then applied a non-dimensional analysis to the model to motivate an analytical stability criterion for the mode transition. We found that this criterion depends on discharge voltage, discharge current, neutral residence time, acceleration zone length, and magnetic field strength. We, in turn, used this result to show that the stability margin—defined as the ability of the thruster to avoid the transition to instability at low discharge currents and fixed discharge voltage—can be changed by adjusting these properties of the thruster.

Physically, we leveraged our derived stability criterion to demonstrate that the critical factor driving the onset of the mode transition is the ratio of the ionization timescale and the neutral transit time. This is consistent with the qualitative interpretation presented in Paper I that the instability is driven unstable by constructive interference between neutral density perturbations in the ionization zone reinforcing ionization in the acceleration zone. We were able to leverage these qualitative insights to inform and demonstrate two mitigation strategies for curtailing the mode transition—adjusting the magnetic field strength and heating the thruster anode. Our work also indicates that reducing channel area for the same current may improve the stability margin.

Critically, the question of why shielded thrusters display more severe mode transitions than unshielded models at high specific impulse and low current may, in part, be explained through the model. Our result demonstrated, for example, how the displacement in the acceleration zone downstream with magnetic shielding may be a driving factor in explaining this difference. We have noted, however, that there are other convolved factors that may contribute to the shifting in the stability margin. Finally, we have discussed how our criterion suggests that thruster stability during qualification and on orbit operation may be critically linked to the thermal state of the thruster.

In summary, the analysis we have performed in this work provides a new tool for assessing mode transitions in Hall thrusters that may be leveraged to not only understand this effect but also develop new designs and mitigation strategies that expand the operating envelope of these devices.

ACKNOWLEDGMENTS

This work was supported through a Strategic University Research Partnership grant from the California Institute of Technology's Jet Propulsion Laboratory. A portion of the research described here was carried out at the Jet Propulsion Laboratory, California Institute of Technology, under a contract with the National Aeronautics and Space Administration (No. 80NM0018D0004).

AUTHOR DECLARATIONS

Conflict of Interest

The authors have no conflicts to disclose.

Author Contributions

Benjamin A. Jorns: Conceptualization (lead); Data curation (equal); Formal analysis (lead); Funding acquisition (equal); Investigation (lead); Methodology (lead); Project administration (equal); Resources (equal); Supervision (lead); Writing – original draft (lead). **Matthew Byrne:** Data curation (supporting); Methodology (supporting). **Parker Roberts:** Data curation (supporting); Investigation (supporting). **Leanne Su:** Investigation (supporting); Methodology (supporting). **Ethan Dale:** Data curation (equal); Formal analysis (supporting); Investigation (supporting). **Richard R. Hofer:** Conceptualization (supporting); Funding acquisition (equal); Investigation (supporting); Project administration (equal); Writing – review & editing (supporting).

DATA AVAILABILITY

The data that support the findings of this study are available from the corresponding author upon reasonable request.

REFERENCES

[1]J. Fife, M. Martinez-Sanchez, J. Szabo, J. Fife, M. Martinez-Sanchez, and J. Szabo, "A numerical study of low-frequency discharge oscillations in Hall thrusters," in *33rd Joint Propulsion Conference and Exhibit, Seattle, WA*, AIAA-1997-3052 (American Institute of Aeronautics and Astronautics, 1997).
[2]J. P. Boeuf and L. Garrigues, "Low frequency oscillations in a stationary plasma thruster," J. Appl. Phys. **84**, 3541–3554 (1998).
[3]S. Barral, V. Lapuerta, A. Sancho, and E. Ahedo, "Numerical investigation of low-frequency longitudinal oscillations in Hall thrusters," in *29th International*

05 August 2024 14:30:42

© Author(s) 2024

Electric Propulsion Conference, Princeton, NJ, IEPC-2005-120 (Electric Rocket Propulsion Society, 2005).
[4]S. Chable and F. Rogier, "Numerical investigation and modeling of stationary plasma thruster low frequency oscillations," Phys. Plasmas **12**, 1–9 (2005).
[5]S. Barral and E. Ahedo, "On the origin of low frequency oscillations in Hall thrusters," AIP Conf. Proc. **993**(1), 439–442 (2008).
[6]S. Barral and Z. Peradzyński, "A new breath for the breathing mode," in *31st International Electric Propulsion Conference, Ann Arbor, MI*, IEPC-2009-070 (Electric Rocket Propulsion Society, 2009).
[7]S. Barral and E. Ahedo, "Low-frequency model of breathing oscillations in Hall discharges," Phys. Rev. E **79**, 46401 (2009).
[8]S. Barral and Z. Peradzyński, "Ionization oscillations in Hall accelerators," Phys. Plasmas **17**, 14505 (2010).
[9]S. Barral and J. Miedzik, "Numerical investigation of closed-loop control for Hall accelerators," J. Appl. Phys. **109**, 013302 (2011).
[10]K. Hara, M. J. Sekerak, I. D. Boyd, and A. D. Gallimore, "Mode transition of a Hall thruster discharge plasma," J. Appl. Phys. **115**, 203304 (2014).
[11]K. Hara, M. J. Sekerak, I. D. Boyd, and A. D. Gallimore, "Perturbation analysis of ionization oscillations in Hall effect thrusters," Phys. Plasmas **21**, 122103 (2014).
[12]O. Koshkarov, A. I. Smolyakov, I. V. Romadanov, O. Chapurin, M. V. Umansky, Y. Raitses, and I. D. Kaganovich, "Current flow instability and nonlinear structures in dissipative two-fluid plasmas," Phys. Plasmas **25**, 011604 (2018).
[13]A. Smolyakov, I. Romadanov, O. Chapurin, Y. Raitses, G. Hagelaar, and J. P. Boeuf, "Stationary profiles and axial mode oscillations in Hall thrusters," in *2019 AIAA Propulsion and Energy Forum and Exposition, Indianapolis*, AIAA-2019-4080 (American Institute of Aeronautics and Astronautics, 2019).
[14]I. V. Romadanov, A. I. Smolyakov, E. A. Sorokina, V. V. Andreev, and N. A. Marusov, "Stability of ion flow and role of boundary conditions in a simplified model of the E × B plasma accelerator with a uniform electron mobility," Plasma Phys. Rep. **46**, 363–373 (2020).
[15]O. Chapurin, A. I. Smolyakov, G. Hagelaar, and Y. Raitses, "On the mechanism of ionization oscillations in Hall thrusters," J. Appl. Phys. **129**, 233307 (2021).
[16]T. Lafleur, P. Chabert, and A. Bourdon, "The origin of the breathing mode in Hall thrusters and its stabilization," J. Appl. Phys. **130**, 053305 (2021).
[17]Y. Esipchuk, A. Morozov, G. Tilinin, and A. Trofimov, "Plasma oscillations in closed-drift accelerators with an extended acceleration zone," Sov. Phys. Tech. Phys. **18**(7), 928–932 (1974).
[18]F. Darnon, M. Lyszyk, A. Bouchoule, F. Darnon, M. Lyszyk, and A. Bouchoule, "Optical investigation on plasma investigations of SPT thrusters," in *33rd Joint Propulsion Conference and Exhibit, Seattle, WA*, AIAA-1997-3051 (American Institute of Aeronautics and Astronautics, 1997).
[19]K. Polzin, E. Scooby, Y. Raitses, E. Merino, and N. J. Fisch, "Discharge oscillations in a permanent magnet cylindrical Hall-effect thruster," in *31st International Electric Propulsion Conference, Ann Arbor, MI*, IEPC-2009-122 (Electric Rocket Propulsion Society, 2009).
[20]R. B. Lobbia, "A time-resolved investigation of the Hall thruster breathing mode," Ph.D. dissertation (University of Michigan, 2010).
[21]M. Sekerak, M. McDonald, R. Hofer, and A. Gallimore, "Hall thruster plume measurements from high-speed dual Langmuir probes with ion saturation reference," in *IEEE Aerospace Conference Proceedings* (IEEE, 2013).
[22]M. S. McDonald and A. D. Gallimore, "Comparison of breathing and spoke mode strength in the H6 Hall thruster using high speed imaging," in *33rd International Electric Propulsion Conference, Washington D.C.*, IEPC-2013-353 (Electric Rocket Propulsion Society, 2013).
[23]M. Sekerak, B. Longmier, A. Gallimore, W. Huang, H. Kamhawi, R. Hofer, B. Jorns, and J. Polk, "Mode transitions in magnetically shielded Hall effect thrusters," in *50th AIAA/ASME/SAE/ASEE Joint Propulsion Conference*, AIAA 2014-3511 (American Institute of Aeronautics and Astronautics, 2014).
[24]C. J. Durot, A. D. Gallimore, and T. B. Smith, "Validation and evaluation of a novel time-resolved laser-induced fluorescence technique," Rev. Sci. Instrum. **85**, 013508 (2014).
[25]A. Lucca Fabris, C. V. Young, and M. A. Cappelli, "Time-resolved laser-induced fluorescence measurement of ion and neutral dynamics in a Hall thruster during ionization oscillations," J. Appl. Phys. **118**, 233301 (2015).
[26]W. Huang, H. Kamhawi, and T. Haag, "Plasma oscillation characterization of NASA's HERMeS Hall thruster via high speed imaging," in *52nd AIAA/SAE/ASEE Joint Propulsion Conference, Salt Lake City, UT*, AIAA-2016-4829 (American Institute of Aeronautics and Astronautics, 2016).
[27]C. V. Young, A. L. Fabris, N. A. Macdonald-Tenenbaum, W. A. Hargus, and M. A. Cappelli, "Time-resolved laser-induced fluorescence diagnostics for electric propulsion and their application to breathing mode dynamics," Plasma Sources Sci. Technol. **27**, 094004 (2018).
[28]I. Romadanov, Y. Raitses, and A. Smolyakov, "Hall thruster with externally driven breathing oscillations," Plasma Sources Sci. Technol. **27**, 094006 (2018).
[29]R. R. Hofer, H. Kamhawi, I. Mikellides, D. Herman, J. Polk, W. Huang, J. Yim, J. Myers, and R. Shastry, "Design methodology and scaling of the 12.5 kW HERMeS Hall thruster for the solar electric propulsion technology demonstration mission," in *62nd JANNAF Propulsion Meeting, Nashville, TN*, JANNAF-2015-3946 (JANNAF Interagency Propulsion Committee, 2015).
[30]R. R. Hofer, J. E. Polk, M. J. Sekerak, I. G. Mikellides, H. Kamhawi, T. R. Sarver-Verhey, D. A. Herman, and G. Williams, "The 12.5 kW Hall effect rocket with magnetic shielding (HERMeS) for the asteroid redirect robotic mission," in *52nd AIAA/SAE/ASEE Joint Propulsion Conference, Salt Lake City, UT*, AIAA-2016-4825 (American Institute of Aeronautics and Astronautics, 2016).
[31]I. G. Mikellides, I. Katz, R. R. Hofer, D. M. Goebel, K. De Grys, and A. Mathers, "Magnetic shielding of the channel walls in a Hall plasma accelerator," Phys. Plasmas **18**, 033501 (2011).
[32]I. G. Mikellides, I. Katz, R. R. Hofer, and D. M. Goebel, "Magnetic shielding of a laboratory Hall thruster. I. Theory and validation," J. Appl. Phys. **115**, 0–20 (2014).
[33]R. R. Hofer, D. M. Goebel, I. G. Mikellides, and I. Katz, "Magnetic shielding of a laboratory Hall thruster. II. Experiments," J. Appl. Phys. **115**, 043304 (2014).
[34]B. Jorns, E. Dale, and R. Hofer, "Mode transitions in a magnetically shielded Hall thruster. I. Experimentally-informed model," J. Appl. Phys. (in press) (2024).
[35]D. M. Goebel and I. Katz, in *JPL Space Science and Technology Series* (John Wiley & Sons, 2008), p. 508.
[36]S. W. Reilly, M. J. Sekerak, and R. R. Hofer, "Transient thermal analysis of the 12.5 kW HERMeS Hall thruster," in *52nd AIAA/SAE/ASEE Joint Propulsion Conference*, AIAA-2016-5024 (American Institute of Aeronautics and Astronautics, 2016).
[37]L. L. Su, P. J. Roberts, T. Gill, W. Hurley, T. A. Marks, C. L. Sercel, M. Allen, C. B. Whittaker, M. Byrne, Z. Brown, E. Viges, and B. Jorns, "Operation and performance of a magnetically shielded Hall thruster at ultrahigh current densities on xenon and krypton," in *AIAA SCITECH 2023 Forum*, AIAA-2023-0842 (American Institute of Aeronautics and Astronautics, 2023).
[38]J.-P. Boeuf, "Tutorial: Physics and modeling of Hall thrusters," J. Appl. Phys. **121**, 11101 (2017).
[39]R. Hofer, S. Cusson, R. Lobbia, and A. Gallimore, "The H9 magnetically shielded Hall thruster," in *35th International Electric Propulsion Conference, Atlanta, GA*, IEPC-2017-232 (Electric Rocket Propulsion Society, 2017).
[40]S. E. Cusson, R. Hofer, R. Lobbia, B. Jorns, and A. Gallimore, 'Performance of the H9 magnetically shielded Hall thrusters,' in *35th International Electric Propulsion Conference, Atlanta, GA*, IEPC-2017-239 (Electric Rocket Propulsion Society, 2017).
[41]E. T. Dale and B. A. Jorns, "Non-invasive characterization of the ionization region of a Hall effect thruster," in *54th AIAA Joint Propulsion Conference, Cincinnati, OH* (American Institute of Aeronautics and Astronautics, 2018), pp. 2018–4508.
[42]E. T. Dale and B. Jorns, "Non-invasive time-resolved measurements of anomalous collision frequency in a Hall thruster," Phys. Plasmas **26**, 013516 (2019).

05 August 2024 14:30:42

© Author(s) 2024

[43]E. T. Dale and B. A. Jorns, "Experimental characterization of Hall thruster breathing mode dynamics," J. Appl. Phys. **130**, 133302 (2021).
[44]S. E. Cusson, E. T. Dale, B. A. Jorns, and A. D. Gallimore, "Acceleration region dynamics in a magnetically shielded Hall thruster," Phys. Plasmas **26**, 023506 (2019).
[45]B. A. Jorns, S. E. Cusson, Z. Brown, and E. Dale, "Non-classical electron transport in the cathode plume of a Hall effect thruster," Phys. Plasmas **27**, 022311 (2020).
[46]L. L. Su and B. Jorns, "Performance at high current densities of a magnetically-shielded Hall thruster," in *2021 AIAA Propulsion and Energy Forum, Virtual*, AIAA-2021-3405 (American Institute of Aeronautics and Astronautics, 2021).
[47]L. L. Su and B. A. Jorns, "Performance comparison of a 9-kW magnetically shielded Hall thruster operating on xenon and krypton," J. Appl. Phys. **130**, 163306 (2021).
[48]E. Viges, B. Jorns, A. Gallimore, and J. Sheehan, "University of Michigan's upgraded large vacuum test facility," in *36th International Electric Propulsion Conference, Vienna*, IEPC-2019-653 (Electric Rocket Propulsion Society, 2019).
[49]J. W. Dankanich, M. Walker, M. W. Swiatek, and J. T. Yim, "Recommended practice for pressure measurement and calculation of effective pumping speed in electric propulsion testing," J. Propul. Power **33**, 668–680 (2017).
[50]E. Y. Choueiri, "Plasma oscillations in Hall thrusters," Phys. Plasmas **8**, 1411–1426 (2001).
[51]B. A. Jorns and R. R. Hofer, "Plasma oscillations in a 6-kW magnetically shielded Hall thruster," Phys. Plasmas **21**, 4–6 (2014).
[52]L. L. Su, T. A. Marks, and B. A. Jorns, "Investigation into the efficiency gap between krypton and xenon operation on a magnetically shielded Hall thruster," in *37th International Electric Propulsion Conference* (Electric Rocket Propulsion Society, Boston, MA, 2022).
[53]E. T. Dale and B. A. Jorns, "Two-zone Hall thruster breathing mode mechanism, Part I: Theory," in *36th International Electric Propulsion Conference, Vienna*, IEPC-2019-354 (Electric Rocket Propulsion Society, 2019).
[54]M. J. Sekerak, A. D. Gallimore, D. L. Brown, R. R. Hofer, and J. E. Polk, "Mode transitions in Hall-effect thrusters induced by variable magnetic field strength," J. Propul. Power **32**, 903–917 (2016).
[55]V. H. Chaplin, B. A. Jorns, A. Lopez Ortega, I. G. Mikellides, R. W. Conversano, R. B. Lobbia, and R. R. Hofer, "Laser-induced fluorescence measurements of acceleration zone scaling in the 12.5 kW HERMeS Hall thruster," J. Appl. Phys. **124**, 183302 (2018).
[56]D. Gawron, S. Mazouffre, N. Sadeghi, and A. Héron, "Influence of magnetic field and discharge voltage on the acceleration layer features in a Hall effect thruster," Plasma Sources Sci. Technol. **17**, 025001 (2008).
[57]W. A. Hargus and M. R. Nakles, "Ion velocity measurements within the acceleration channel of a low-power Hall thruster," IEEE Trans. Plasma Sci. **36**, 1989–1997 (2008).
[58]M. R. Nakles and W. A. Hargus, "Background pressure effects on ion velocity distribution within a medium-power Hall thruster," J. Propul. Power **27**, 737–743 (2011).
[59]C. F. Book and M. L. R. Walker, "Effect of anode temperature on Hall thruster performance," J. Propul. Power **26**, 1036–1044 (2010).
[60]E. T. Dale, B. Jorns, and K. Hara, "Numerical investigation of the stability criteria for the breathing mode in Hall effect thrusters," in *35th International Electric Propulsion Conference, Atlanta, GA*, IEPC-2017-265 (Electric Rocket Propulsion Society, 2017).
[61]W. A. Hargus and B. Pote, "Examination of a Hall thruster start transient," in *38th AIAA/ASME/SAE/ASEE Joint Propulsion Conference and Exhibit*, AIAA-2002-3956 (American Institute of Aeronautics and Astronautics, 2002).

05 August 2024 14:30:42

© Author(s) 2024